

Supplementary Material for “A Majorize-Minimize Framework for the Statistical Processing of Non-Central Chi MR Images”

Divya Varadarajan, *Student Member, IEEE*, Justin P. Haldar, *Member, IEEE*

This supplement contains additional material to complement the results presented in the main body of the paper. Proofs of Theorems 1 and 2 are given in Secs. I and II, respectively, while supplementary figures are found in Sec. III.

I. PROOF OF THEOREM 1

The NCC NLL in (7) is the sum of functions of the form

$$L(t) = \frac{t^2}{2\sigma^2} - \ln\left(t^{-(N-1)} I_{N-1}(t\gamma/\sigma^2)\right). \quad (\text{S1})$$

Our proof of Theorem 1 is based on tangent majorization of the function $L(t)$, which is easily decomposed into the strictly convex quadratic term $t^2/(2\sigma^2)$ and the strictly concave (cf. Theorem 2) log-Bessel term $\ell(t) \triangleq -\ln\left(t^{-(N-1)} I_{N-1}(t\gamma/\sigma^2)\right)$.

Differentiable concave functions can always be majorized by their tangents [1]. This means that, for any t_i ,

$$\ell(t) \leq \ell(t_i) + \nabla\ell(t_i)(t - t_i), \quad (\text{S2})$$

such that

$$L(t) \leq \frac{t^2}{2\sigma^2} + \ell(t_i) + \nabla\ell(t_i)(t - t_i) \triangleq \tilde{L}(t|t_i). \quad (\text{S3})$$

Eq. (S3), combined with the fact that $\tilde{L}(t_i|t_i) = L(t_i)$, implies that $\tilde{L}(t|t_i)$ is a tangent majorizer for $L(t)$ at the point t_i .

Completing the square in (S3) leads to

$$\tilde{L}(t|t_i) = \frac{1}{2\sigma^2} (t + \sigma^2 \nabla\ell(t_i))^2 + K_i, \quad (\text{S4})$$

where

$$K_i = \ell(t_i) - t_i \nabla\ell(t_i) - \frac{\sigma^2}{2} (\nabla\ell(t_i))^2. \quad (\text{S5})$$

It remains to derive the form of the gradient $\nabla\ell(t)$. Straightforward application of the chain rule yields that

$$\nabla\ell(t) = -\frac{\frac{\partial}{\partial t} \{t^{-(N-1)} I_{N-1}(t\gamma/\sigma^2)\}}{t^{-(N-1)} I_{N-1}(t\gamma/\sigma^2)}. \quad (\text{S6})$$

Using the identity for modified Bessel functions [2, Sec. 9.6]:

$$\frac{\partial(t^{-v} I_v(t))}{\partial t} = t^{-v} I_{v+1}(t), \quad (\text{S7})$$

we have that Eq. (S6) simplifies to

$$\nabla\ell(t) = -\frac{\gamma}{\sigma^2} \frac{I_N(t\gamma/\sigma^2)}{I_{N-1}(t\gamma/\sigma^2)}. \quad (\text{S8})$$

As a result, $\tilde{L}(t|t_i)$ can be expressed as

$$\tilde{L}(t|t_i) = \frac{1}{2\sigma^2} \left(t - \gamma \frac{I_N(t\gamma/\sigma^2)}{I_{N-1}(t\gamma/\sigma^2)} \right)^2 + K_i. \quad (\text{S9})$$

The proof of Theorem 1 is concluded by directly applying the corresponding $\tilde{L}(t|t_i)$ majorizer from (S9) to each of the M different summands in (9). \square

II. PROOF OF THEOREM 2

Theorem 2 was proven for the special case of $N = 0$ in [3, Cor. 2]. For $N > 0$, we have from [3] that

$$\begin{aligned} I_N(\alpha x) &= \frac{(\alpha x/2)^N}{\Gamma(1+N)} {}_0F_1(1+N; \alpha^2 x^2/4) \\ &= \frac{(\alpha x/2)^N}{\Gamma(1+N)} t_N(\alpha x), \end{aligned} \quad (\text{S10})$$

where $\Gamma(\cdot)$ is the Gamma function, and $t_N(x)$ denotes the hyper-geometric function ${}_0F_1(1+N; x^2/4)$. Eq. (S10) immediately leads to

$$\begin{aligned} \ln(x^{-N} I_N(\alpha x)) &= \ln\left(\frac{(\alpha/2)^N}{\Gamma(1+N)} t_N(\alpha x)\right) \\ &= \ln\left(\frac{(\alpha/2)^N}{\Gamma(1+N)}\right) + \ln(t_N(\alpha x)). \end{aligned} \quad (\text{S11})$$

It was proven in [3, Prop. 1] that $\ln(t_N(x))$ is a strictly convex function of x for $N \geq 0$, which implies that $\ln(t_N(\alpha x))$ is also strictly convex for $\alpha > 0$. Noting that $\ln\left(\frac{(\alpha/2)^N}{\Gamma(1+N)}\right)$ is constant, we have that $\log(x^{-N} I_N(\alpha x))$ is also strictly convex. Therefore, $-\ln(x^{-N} I_N(\alpha x))$ is strictly concave. \square

REFERENCES

- [1] D. R. Hunter and K. Lange, “A tutorial on MM algorithms,” *Am. Stat.*, vol. 58, pp. 30–37, 2004.
- [2] M. Abramowitz and I. A. Stegun, Eds., *Handbook of Mathematical Functions with Formulas, Graphs, and Mathematical Tables*, 10th ed., ser. NBS Applied Mathematics Series 55. Washington, DC: National Bureau of Standards, 1972.
- [3] E. Neuman, “Inequalities involving modified Bessel functions of the first kind,” *J. Math. Anal. Appl.*, vol. 171, pp. 532–536, 1992.

III. SUPPLEMENTARY FIGURES

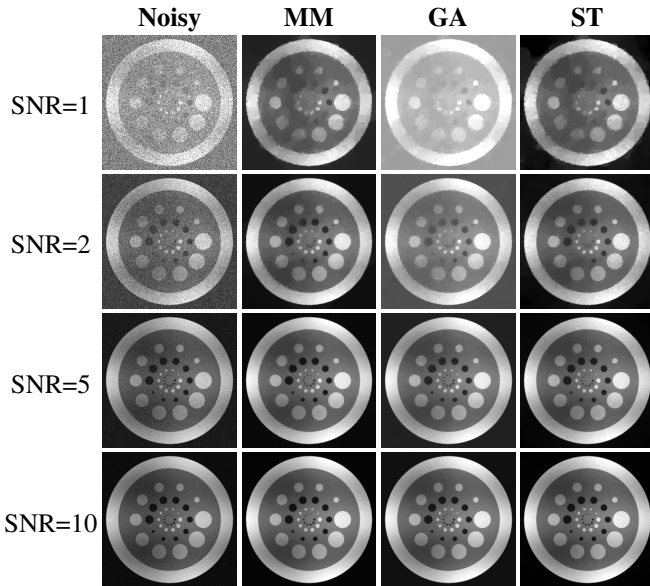


Fig. S1: Representative results from TV denoising of simulated rSoS ($N = 4$) data.

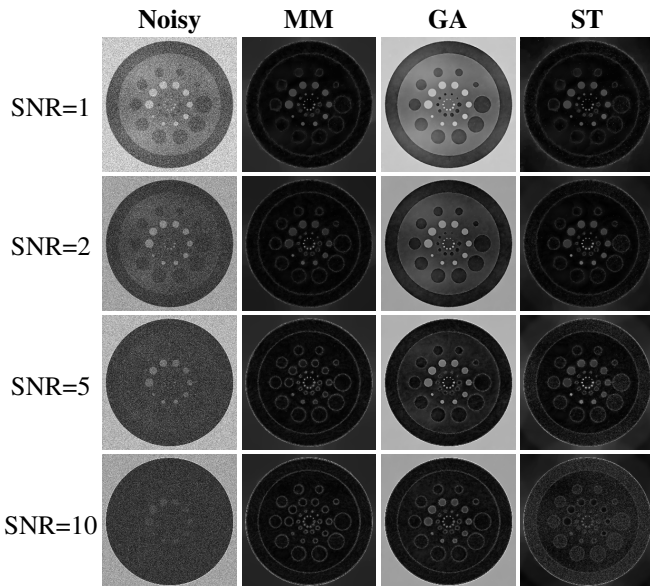


Fig. S2: Root-mean-squared error images (computed based on five noise realizations) for the rSoS TV denoising results shown in Fig. S1. For easier visualization, the error intensities for SNRs 1, 2, 5, and 10 were respectively scaled by factors of 1.25, 2, 5.56, and 10 relative to the images in Fig. S1.

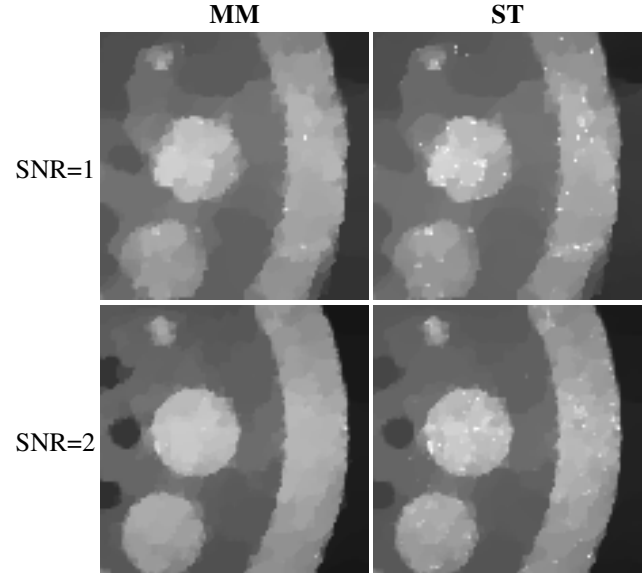


Fig. S3: Zoomed regions from Fig. 2, highlighting the relatively uniform smoothing achieved by MM-based TV denoising and the intensity-dependent smoothing achieved by ST-based TV denoising. Notice that the ST results have a more “speckled” appearance in higher-intensity image regions, but are quite smooth in low-intensity image regions.

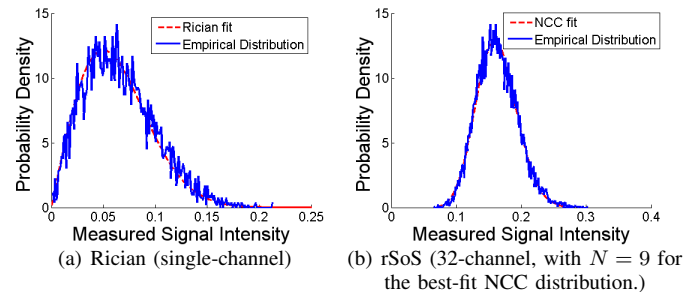


Fig. S4: Empirical distributions of the signal intensity from background regions of real MR brain data. Best-fit Rician and NCC distributions are also shown.

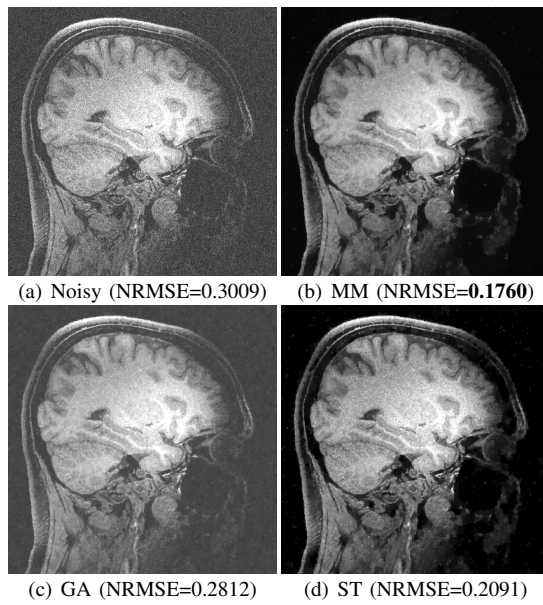


Fig. S5: Results from TV denoising of real rSoS brain data. Also shown are the NRMSE values for each image.

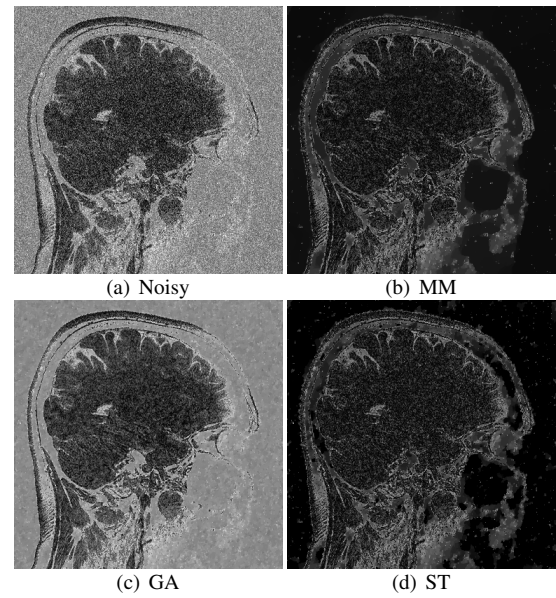


Fig. S6: Error images for the rSoS TV denoising results shown in Fig. S5. For easier visualization, the error image intensities were scaled by a factor of 2 relative to the images in Fig. S5.

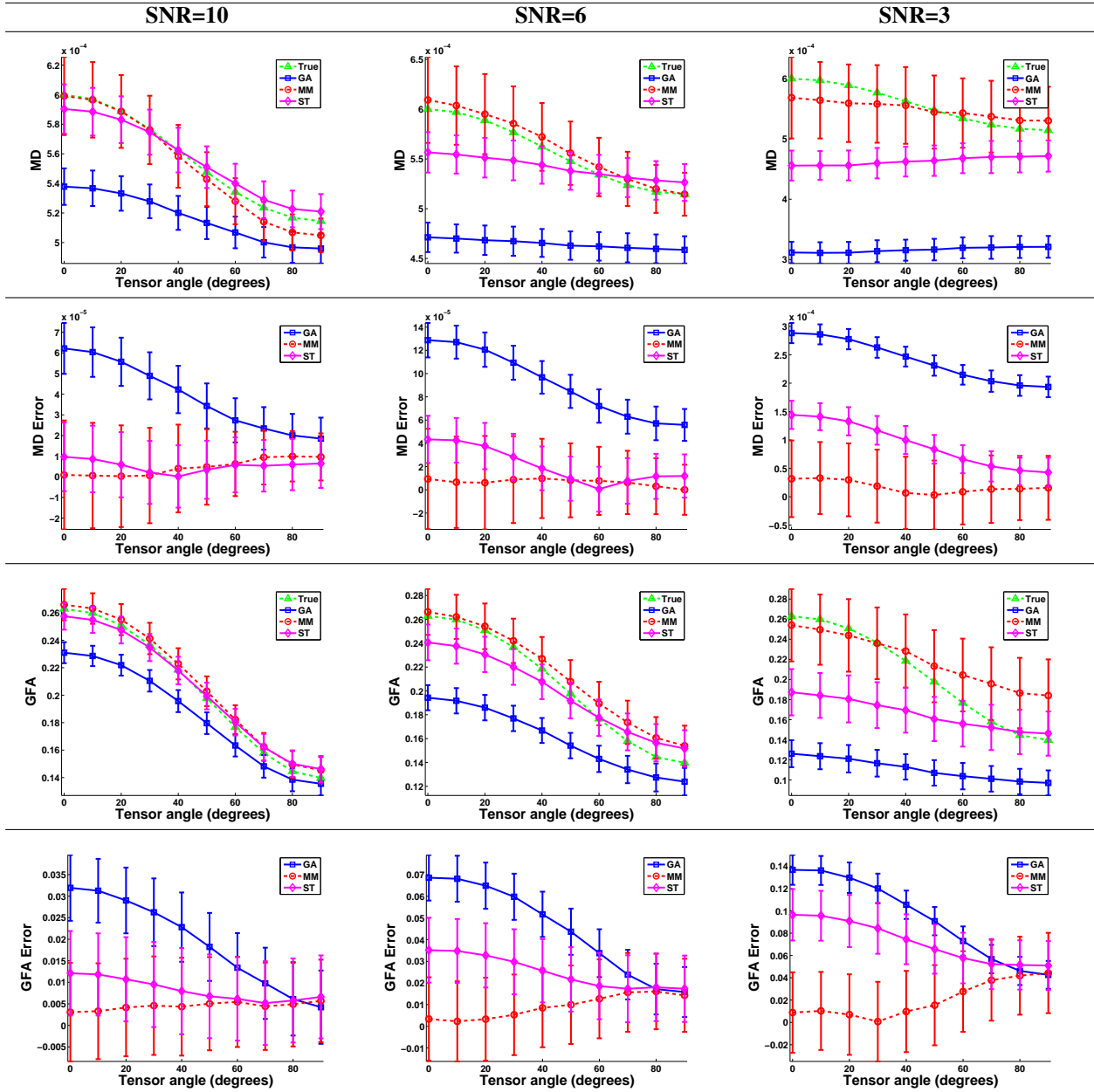


Fig. S7: Quantitative MD and GFA estimation results for the HARDI simulations. In addition to MD and GFA, plots are also included that show the absolute errors for MD and GFA. The lines and error bars respectively correspond to the means and standard deviations across 1000 noise realizations.

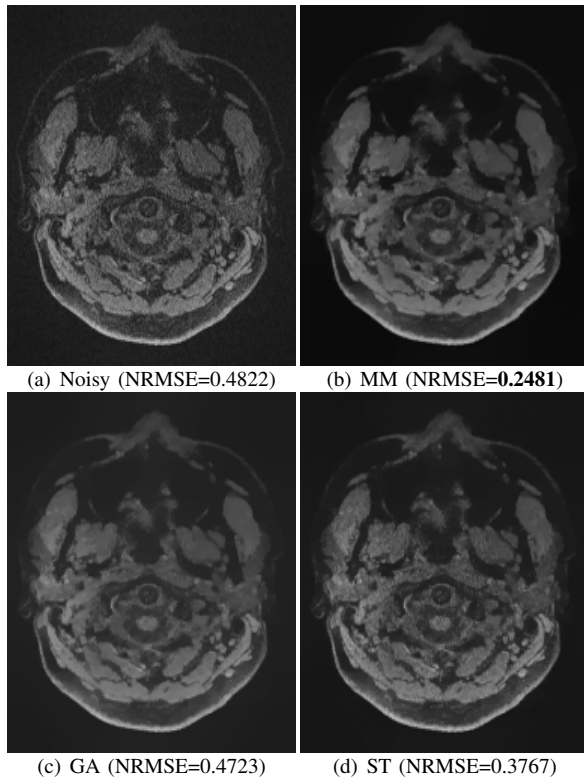


Fig. S8: Results from TV denoising of real GRAPPA-reconstructed rSoS-combined brain data. Also shown are the NRMSE values for each image.

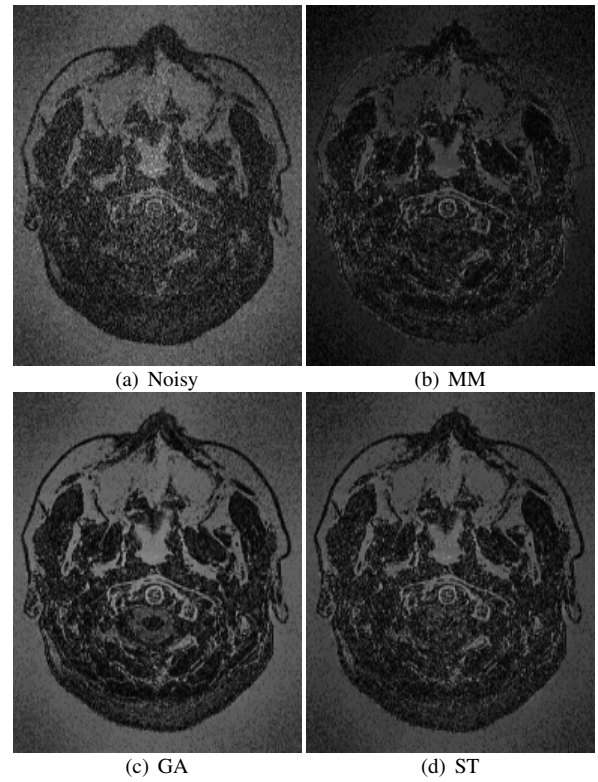


Fig. S9: Error images for the TV denoising results shown in Fig. S8. For easier visualization, the error image intensities were scaled by a factor of 3 relative to the images in Fig. S8.